Received: 2 April 2020 | Revised: 2 September 2020 | Accepted: 5 September 2020

DOI: 10.1002/hipo.23265

WILEY

RESEARCH ARTICLE

Environmental deformations dynamically shift human spatial memory

Alexandra T. Keinath[1†] | Ohad Rechnitz[2†] | Vijay Balasubramanian[3] | Russell A. Epstein[1]

[1]Department of Psychology, University of Pennsylvania, Philadelphia, Pennsylvania

[2]Rappaport Faculty of Medicine and Research Institute, Technion – Israel Institute of Technology, Haifa, Israel

[3]Department of Physics, University of Pennsylvania, Philadelphia, Pennsylvania

Correspondence
Alexandra T. Keinath, Department of Psychology, University of Pennsylvania, Philadelphia, PA.
Email: atkeinath@gmail.com

Funding information
Honda Research Institute Curious-Minded Machines; National Institutes of Health, Grant/Award Numbers: EY022350, EY027047; National Science Foundation, Grant/Award Numbers: IGERT 0966142, PHY-1607611, PHY-1734030

Abstract

Place and grid cells in the hippocampal formation are commonly thought to support a unified and coherent cognitive map of space. This mapping mechanism faces a challenge when a navigator is placed in a familiar environment that has been deformed from its original shape. Under such circumstances, many transformations could plausibly serve to map a navigator's familiar cognitive map to the deformed space. Previous empirical results indicate that the firing fields of rodent place and grid cells stretch or compress in a manner that approximately matches the environmental deformation, and human spatial memory exhibits similar distortions. These effects have been interpreted as evidence that reshaping a familiar environment elicits an analogously reshaped cognitive map. However, recent work has suggested an alternative explanation, whereby deformation-induced distortions of the grid code are attributable to a mechanism that dynamically anchors grid fields to the most recently experienced boundary, thus causing history-dependent shifts in grid phase. This interpretation raises the possibility that human spatial memory will exhibit similar history-dependent dynamics. To test this prediction, we taught participants the locations of objects in a virtual environment and then probed their memory for these locations in deformed versions of this environment. Across three experiments with variable access to visual and vestibular cues, we observed the predicted pattern, whereby the remembered locations of objects were shifted from trial to trial depending on the boundary of origin of the participant's movement trajectory. These results provide evidence for a dynamic anchoring mechanism that governs both neuronal firing and spatial memory.

KEYWORDS

boundaries, environmental deformations, grid cells, human spatial memory, place cells, virtual reality

1 | INTRODUCTION

The hippocampal formation maintains a representation of space through the coordinated activity of a variety of functionally distinct cells types. Among the most well-characterized of these cell types are place cells and grid cells. Place cells are sparsely active cells in the hippocampus that are tuned to different preferred locations (O'Keefe & Dostrovsky, 1971), while grid cells are broadly active cells in medial entorhinal cortex that are tuned to a hexagonal lattice of preferred locations that tessellate the navigable space (Hafting, Fyhn, Molden,

[†] Alexandra T. Keinath and Ohad Rechnitz contributed equally to this work.

Moser, & Moser, 2005). According to a longstanding hypothesis, these cells support a "cognitive map," which, in the classical formulation, consists of a Euclidean coordinate system that allows a navigator to define locations in space and the distances and directions between them (O'Keefe & Nadel, 1978). Consistent with this idea, many theoretical papers have explored how place and grid cells might support the elements of map-based navigation, including self-localization, vector computation, and flexible route planning (Burak & Fiete, 2009; Bush, Barry, Manson, & Burgess, 2015; Fiete, Burak, & Brookings, 2008; McNaughton, Battaglia, Jensen, Moser, & Moser, 2006).

For a cognitive map (or any spatial representation) to be useful, it must be anchored to the environment (Epstein, Patai, Julian, & Spiers, 2017; Gallistel, 1990). The geometry of the environment as defined by environmental boundaries has been found to play a particularly crucial role in anchoring the firing fields of place and grid cells. For example, place and grid fields orient to the walls of experimental chambers (Keinath, Julian, Epstein, & Muzzio, 2017; Krupic, Bauza, Burton, Barry, & O'Keefe, 2015; Weiss et al., 2017), and grid lattices exhibit characteristic inhomogeneities that are related to chamber geometry in square (Stensola, Stensola, Moser, & Moser, 2015) and trapezoidal (Krupic et al., 2015) environments. Moreover, when a familiar environment is reshaped, for example by moving the boundaries so that the environment is stretched or compressed along one-dimension, place and grid fields are distorted in stereotyped ways (Barry, Hayman, Burgess, & Jeffery, 2007; Krupic, Bauza, Burton, & O'Keefe, 2018; McNaughton et al., 1996; O'Keefe & Burgess, 1996; Stensola et al., 2012): stretching or compressing the environment causes the grid pattern of some cells to stretch or compress to match the deformation (Barry et al., 2007; Savelli, Yoganarasimha, & Knierim, 2008; Stensola et al., 2012) (Figure 1a), and stretching causes the preferred locations of place cells to stretch and/or bifurcate (O'Keefe & Burgess, 1996). These results demonstrate that environmental boundaries can act as anchors that influence the locations and shapes of place and grid fields.

Notably, analogous effects of environmental geometry have been observed in human spatial memory (Bellmund et al., 2020; Chen, He, Kelly, Fiete, & McNamara, 2015; Hartley, Trinkler, & Burgess, 2004). For example, when human participants are asked to replace objects in remembered locations in a trapezoidal virtual environment, or to estimate distances between these objects, they make errors that mirror the distortions that are observed in rodent grid fields (Bellmund et al., 2020). Similarly, when human participants are asked to replace objects at learned locations in rescaled virtual environments, their responses form a distribution that is stretched and/or bifurcated, similar to the responses of rodent place cells (Hartley et al., 2004; O'Keefe & Burgess, 1996), and when they are asked to estimate their own locations, their responses are biased in ways that are consistent with the observed rescaling of the grid code (Barry et al., 2007; Chen et al., 2015). The striking concordance between the influence of environmental boundaries on both neural recordings and navigation behavior suggests that in this particular instance, both approaches may assay similar components of cognition. This similarity is especially surprising given the limited scope of neural recordings relative to the scale of the brain producing the behavior, and the many cases in which insights gleaned from subsets of these neural representations fail to generalize to behavior both within and across species (Ekstrom, Harootonian, & Huffman, 2020; Jeffery, Gilbert, Burton, & Strudwick, 2003; Krakauer, Ghazanfar, Gomez-Marin, MacIver, & Poeppel, 2017; Warren, 2019; Zhao, 2018).

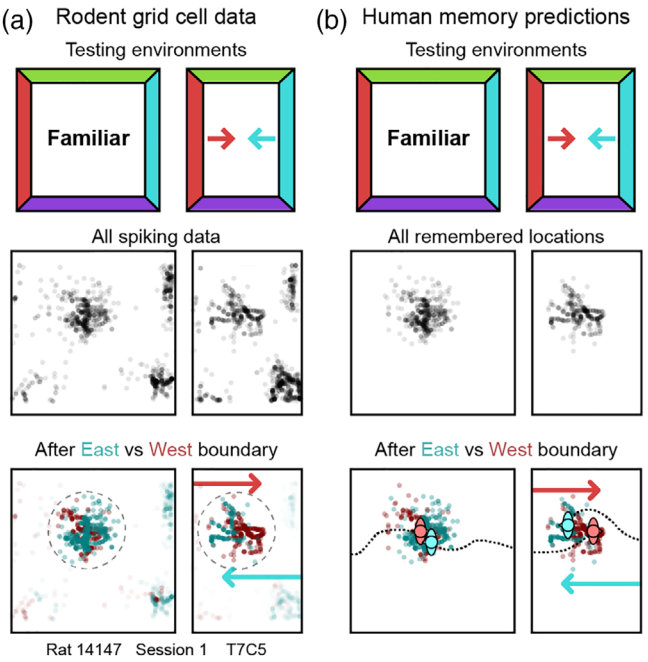

FIGURE 1 Boundary-anchored shifts in grid phase predict boundary-anchored shifts in human spatial memory. (a) Schematic of testing environments, a whole-trial rate map, and spiking locations from an example grid cell. When data from the whole trial are pooled together, the grid pattern appears to rescale (middle). When the data are divided according to the most recently contacted boundary (east vs. west), shifts in preferred locations become apparent (bottom). These shifts act to preserve the distance between the familiar field location and the most recently contacted boundary. Data from (Stensola et al., 2012), reanalysis from (Keinath, Epstein, & Balasubramanian, 2018). (b) Schematic of testing environments and predicted remembered locations when human participants are asked to repeatedly replace an object following contact with each boundary (east vs. west). Analogous to shifts in grid phase, we predict shifts in remembered locations which act to preserve the distance between the learned object location and the most recently contacted boundary [Color figure can be viewed at wileyonlinelibrary.com]

Together, these results have been taken to indicate that the cognitive map is at least partially malleable depending on the geometry of the environment (Barry et al., 2007; Ocko, Hardcastle, Giocomo, & Ganguli, 2018). For example, when a familiar environment is deformed, the navigator's internal representation of space is believed to be stretched or compressed to fit the dimensions of the reshaped environment, possibly due to recalibration of velocity estimation/path integration or local visual input (Bush & Burgess, 2014; Jayakumar et al., 2019; Munn, Mallory, Hardcastle, Chetkovich, & Giocomo, 2020; Ocko et al., 2018; Raudies & Hasselmo, 2015; Sheynikhovich, Chavarriaga, Strösslin, Arleo, & Gerstner, 2009).

However, there are other possible explanations for the rescaling effects that are observed during environmental deformations (Cheung, Ball, Milford, Wyeth, & Wiles, 2012; Keinath et al., 2018). Under one such alternative account, the apparent distortions observed in spatial firing fields and spatial memory during environmental deformations reflect a history-dependent process by which grid phase is dynamically anchored to recently experienced boundaries and subsequently updated via self-motion information (Cheung et al., 2012; Hardcastle, Ganguli, & Giocomo, 2015; Keinath et al., 2018; Savelli, Luck, & Knierim, 2017). During deformations, such anchoring would cause shifts in grid phase which preserve the familiar relationship between grid phase and the most recently contacted boundary. These shifts would appear as distortions in the time-averaged grid fields, even if the spatial metric is in fact maintained relative to the most-recently contacted wall (Figure 1a). At an algorithmic level, this account claims that a navigator self-localizes via path integration which is reset when a familiar boundary is encountered. In deformed environments, this dynamic anchoring predicts the existence of biases in self-localization that are incommensurate when the navigator begins trajectories originating from opposing displaced boundaries. Such biases in self-localization might be reflected in spatial memory during active navigation to a remembered location (Figure 1b).

In a previous report, we provided neural and modeling evidence for boundary-dependent shifts in grid phase that contribute to the appearance of a rescaled time-averaged grid pattern during environmental deformations (Keinath et al., 2018). Evidence of dynamic shifts in grid phase has also been observed in virtual environmental deformations (Chen, Lu, King, Cacucci, & Burgess, 2019). Here we test whether such dynamic anchoring may also be observed in human spatial memory during environmental deformations. Participants in the current experiments learned the locations of objects within square virtual environments. At test, they were asked to walk to the remembered locations of these objects. Unbeknownst to the participants, the environments at test were stretched or compressed along one-dimension. We predicted that the replace locations would be shifted along the deformed axis, with the direction of the shift dependent on the boundary of origin. We found that this prediction was confirmed in three separate experiments under variable visual and vestibular conditions, using both desktop and immersive virtual reality (VR). These results strengthen the link between hippocampal spatial representations and spatial memory during environmental deformations, and provide specific evidence in favor of a dynamic-anchoring mechanism that governs self-localization within rodent spatial representations and human spatial memory alike.

2 | RESULTS

2.1 | Experiment 1: Desktop virtual environment with full visual information available

First, we tested whether human spatial memory is biased by boundary of origin when a familiar environment is deformed and localizing visual information is available. To this end, we used desktop virtual reality (VR) to test participants' memory of the locations of four nameable objects in a room, with a design adapted from previous studies (Doeller & Burgess, 2008) (Figures 2 and S1a). Participants learned the locations of these objects by "collecting" them one at a time, and then demonstrated their spatial memory by "replacing" them in their remembered locations. In "collect" trials, one of the four objects was visible in the room. Participants started in a random location within the environment and navigated to the object. In "replace" trials, no objects were visible in the room. Participants were given the name of one of the four objects and navigated to its remembered location, starting from an initial position close to and facing the center of one of the walls.

The experiment was composed of two blocks. Each block began with eight "collect" trials, followed by a sequence of 16 trial pairs consisting of a "replace" trial immediately followed by a "collect" trial (which served to provide feedback about the correct location for that object). In the replace-collect sequence, each object was replaced four times, starting each time from a position facing the middle of a different wall (North, South, East, West; NSEW). During the first block, the environment remained undeformed throughout all trials. During the second block, the environment was either stretched (n = 24 participants) or compressed (n = 24 participants; randomly assigned) during replace trials by increasing/decreasing the length of the walls by 50% along one axis (Figure 2). The floor, wall, and ceiling textures were not rescaled, but were instead truncated (during compressions) or continued to tile the new space (during stretches). To ensure that participants only learned the locations of objects in their undeformed familiar locations, the environment was never deformed during collect trials. No differences in Block 1 accuracy (distance from correct location, mean ± SEM, stretched: 29.42 ± 2.09 virtual units, v.u.; compressed: 30.13 ± 1.48 v.u.; Wilcoxon rank sum test, two-tailed: W = 607, p = .703) or reaction time (stretched: 16.14 ± 1.13 s; compressed: 15.46 ± 1.99 s; Wilcoxon rank sum test, two-tailed: W = 519, p = .158) were observed between participants assigned to the stretched versus compressed conditions, indicating that both groups learned the task equally well.

We hypothesized that during the deformation block replace locations of an object would be shifted to bias this location in the direction that best preserves the learned distance between the familiar object location and the starting boundary in each trial (Figure 1b). Thus, we predicted that, in a stretched environment, the replace locations in individual trials would be shifted toward the boundary of origin of the navigator's trajectory, as compared with the median replaced location. Likewise, we predicted that in a compressed environment the replace location in individual trials would be shifted away from the boundary of origin, as compared to the median replaced location.

To test this prediction, we performed the following calculation (Figure 3). First, we aligned the median replace locations ignoring boundary of origin across the four objects. Next, we broke down these aligned data based on the boundary of origin (NSEW) and calculated the median replace location separately for each boundary.

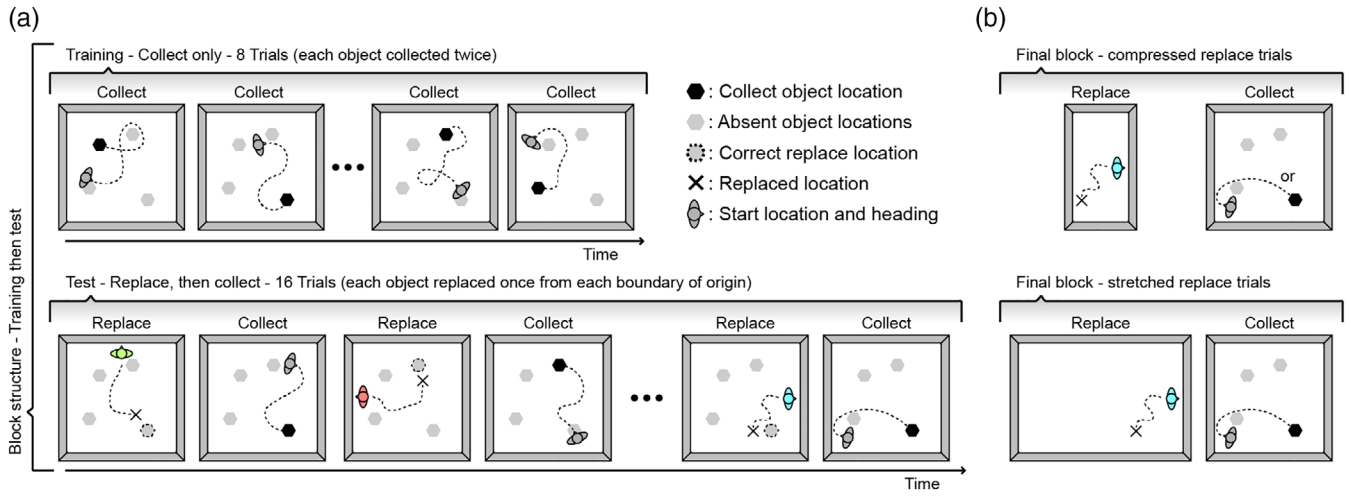

FIGURE 2 Experimental design. (a) Schematic of block structure. Each block began with participants collecting each of the four objects two times starting from randomly assigned starting locations (Training). Next, participants replaced every object four times, once each from an initial starting location at the middle of each boundary, facing that boundary. (b) Schematic of environmental deformations during the replace trials of the final block of each experiment. Only replace trials differed between blocks. During the replace trials of initial block(s) the environment remained undeformed. During replace trials of the final block, the environment was either stretched or compressed [Color figure can be viewed at wileyonlinelibrary.com]

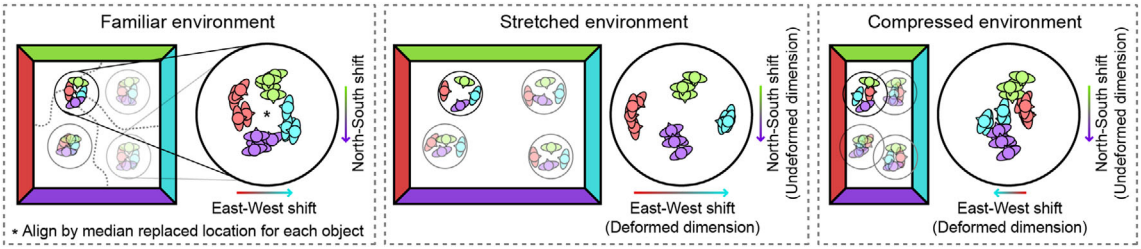

FIGURE 3 Schematic of analysis. To quantify shifts in the replace locations of objects depending on recently experienced boundaries, we first aligned the median replace locations across the four objects. Next, for each axis we calculated shift as the displacement along that axis between the median aligned replace locations when the participant started from a given boundary versus the opposing boundary. For example, to quantify east–west shift we computed the median replace location when the participant started from the west minus when the participant started from the east, ignoring any shift along the north–south axis. Shift was then compared between deformed and undeformed dimensions during deformation blocks. Note that the direction of predicted shift differs between stretched and compressed deformations [Color figure can be viewed at wileyonlinelibrary.com]

Finally, we calculated shift along each axis as the displacement between replace locations with opposing boundaries of origin along that axis. For example, to quantify EW (NS) shift we computed the median replace location of aligned west (south) boundary of origin trials minus aligned east (north) boundary of origin trials, ignoring any shift along the NS (EW) axis. Finally, we computed the difference in shift between the deformed (EW) and undeformed (NS) dimensions. With these conventions, the boundary-anchoring account predicts that an East–West (North–South) stretching of the environment should lead to a positive shift difference in the replace locations, while a compression should lead to a negative shift difference.

During the deformation block, we indeed observed a positive shift difference for replace trials in the stretched environment (Wilcoxon signed rank test vs. 0, one-tailed: W = 232, p = .0096) and a negative shift difference for replace trials in the compressed environment (Wilcoxon signed rank test vs. 0, one-tailed: W = 61, p = .0055). The difference in shift difference between the two environments was significant (Wilcoxon rank sum test, one-tailed: W = 426, p = .0009; Figures 4 and S2a). The two environments did not differ in shift along the undeformed dimension (Wilcoxon rank sum test: W = 653, p = .1835). Thus, replace locations in the deformed environments were shifted depending on the boundary of origin, as predicted by a boundary anchoring account.

Notably, participants tended to face away from the boundary of origin when replacing objects (Figure S3). If participants determined their replace locations based on visual perception of the distance to the dominant visual boundary at the time of object replacement, then the inverse pattern of shift differences would be predicted (positive

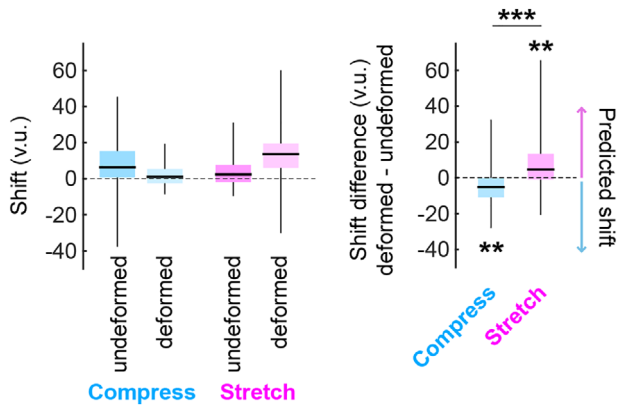

FIGURE 4 Deformations induce path-dependent shifts in human spatial memory. Shift along each axis for each condition (left) and shift difference between deformed and undeformed dimensions (right) from Experiment 1: Desktop virtual environment with full visual information available. The vertical axis is in virtual units (v.u.). Shift along each axis was positive indicating that participants generally tended to underestimate distances when navigating to replace the objects, as has been observed previously (Chen et al., 2015; Thompson et al., 2004). Colored arrows indicate the direction of shift difference predicted for each condition. Significance markers denote the outcome of nonparametric Wilcoxon signed rank (one-tailed in predicted directions) and rank sum tests. $^{**}p < .01$, $^{***}p < .001$ [Color figure can be viewed at wileyonlinelibrary.com]

shift difference in the compressed environment; negative shift difference in the stretched environment). Thus, it is unlikely that the shifts in object replace locations we observed were attributable to anchoring of the replace location to the dominant visual boundary at the point of replacement, rather than anchoring to the boundary from which the navigational episode began. Nevertheless, due to biased sampling of dominant visual boundaries at the time of object replacement (Figure S3), we were unable to apply the same shift analysis to explicitly rule out this alternative account. We address this possibility directly in Experiment 2 by manipulating the availability of visual boundaries during object replacement.

The crucial part of our approach is that we analyzed the data separately for each boundary of origin. When the data were analyzed without regard to the boundary of origin, the pattern of replace locations during deformation blocks resembled a rescaling of the familiar object locations that qualitatively matched the rescaling of the environment (Figure S4), similar to previous results (Chen et al., 2015; Hartley et al., 2004). Thus, a static coordinate transformation that maps familiar object locations to deformed replace locations does capture the general pattern of object replace locations in the mean data. However, it cannot account for the path-dependent dynamics we observe.

Together, these results indicate that human spatial memory is dynamically anchored to the boundary of origin in deformed environments when full visual information is available. Participants tend to recapitulate the distance of the object from the starting boundary, even though this means that they replace the object in inconsistent locations within the deformed room.

2.2 | Experiment 2: Desktop virtual environment with visual information obscured during replace trials

At an implementation level, dynamic phase-anchoring of the grid code during environmental deformations is thought to reflect a path integration mechanism which is reset when a familiar boundary is experienced (Cheung et al., 2012; Keinath et al., 2018). Alternatively, some models posit that the effects of environmental deformations on spatial representations and memory reflect changes to self-localization estimates derived from continuous visual input from boundaries (Raudies & Hasselmo, 2015; Sheynikhovich et al., 2009). To explicitly test whether the dynamic anchoring of human spatial memory to boundary of origin depends on continuous visual access to boundaries, we probed human spatial memory during deformations when this visual information was unavailable.

To this end, we used desktop VR to test a new cohort of participants on the locations of four nameable objects in a room. The design was similar to the first experiment (Figure 2). The experiment comprised three blocks. Each block began with 8 "collect" trials, followed by a sequence of 16 trial pairs consisting of a "replace" trial immediately followed by "collect" trial for the replaced object. Each object was replaced four times in this replace-collect sequence, with each replace trial starting from a position facing the middle of one of the four wall. During the first block, all trials were conducted with full visual information available (Figure S1b). In the second and third block, visual cues during the collect trials were visible, but visual cues during replace trials were obscured by a dense fog once the participant moved from her starting location (Figure S1b). This fog made it impossible for the participant to see anything beyond what was immediately in front of her (within 12.5 v.u., about 10% the length of the familiar environment). In most parts of the environment, this meant that only the floor was visible, which provided optic flow information but no cues to environment rescaling. To perform the task accurately under these conditions, participants needed to plan their path at the beginning of the trial before the fog appeared and to keep track of where they were while moving. The undeformed environment was used for all trials in blocks 1 and 2, and for collect trials in block 3. For replace trials in block 3, the environment was either stretched (n = 24 participants) or compressed (n = 24 participants; randomly assigned) by 50% along one axis during all replace trials. The floor, wall, and ceiling textures were not rescaled, but were instead truncated (during compressions) or continued to tile the new space (during stretches). No differences in Block 2 accuracy (distance from correct location, mean ± SEM; stretched: 25.87 ± 1.90 v.u.; compressed: 26.17 ± 1.52 v.u.; Wilcoxon rank sum test, two-tailed: W = 608, p = .688) or reaction time (stretched: 15.25 ± 1.47 s; compressed: 13.67 ± 1.37 s; Wilcoxon rank sum test, two-tailed: W = 534.5, p = .274) were observed between participants assigned to the stretched versus compressed conditions, indicating that both groups learned the task equally well.

Similar to the results of our first experiment, and matching the predictions of a dynamic anchoring account, we again observed a positive shift difference for replace trials in the stretched environment

(Wilcoxon signed rank test vs. 0, one-tailed: W = 275, p = .0002) and a negative shift difference for replace trials in the compressed environment (Wilcoxon signed rank test vs. 0, one-tailed: W = 72, p = .0129), with a significant difference between these deformations (Wilcoxon rank sum test, one-tailed: W = 382, p = .00002; Figures 5 and S2b). No significant difference in shift along undeformed dimensions was observed between stretched and compressed environments (Wilcoxon rank sum test: W = 542, p = .3481).

As in Experiment 1, participants on average tended to face away from the boundary of origin when replacing objects (Figure S3). Due to this in combination with learned object locations being far from walls (>30v.u.) and the visibility restrictions due to the dense fog during replacement (complete occlusion at 12.5 v.u.), walls were rarely visible at the time of object replacement. Indeed, during both stretched and compressed blocks all boundaries were completely obscured to the participant during the much of the replacement trial after her initial movement (compressed: 49.3 ± 1.5% of trial; stretched: 60.0 ± 1.3% of trial; mean ± SEM across trials), and were not visible at the time of object replacement on the vast majority of trials (compressed: 364 of 384, 94.8%; stretched: 364 of 384, 94.8%). Thus anchoring to dominant visual boundaries at the time of object replacement cannot explain the pattern of shift differences we observe in this experiment. Moreover, comparing these results to those of Experiment 1 in which the deformations, apparatus, and object locations were comparable, the magnitude of shift differences was numerically larger on average during replacement in dense fog

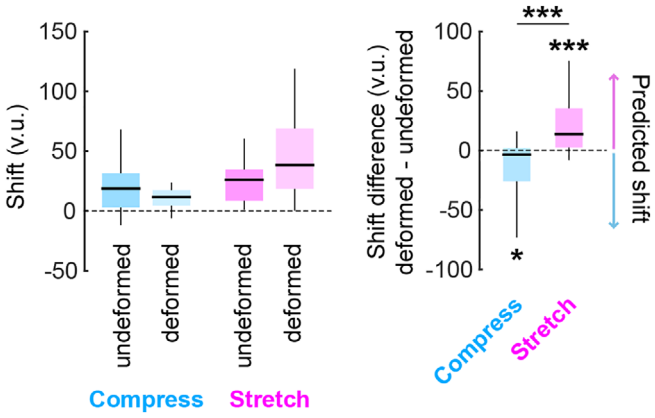

FIGURE 5 Deformations induce path-dependent shifts in human spatial memory when localizing visual information is obscured. Shift along each axis for each condition (left) and shift difference between deformed and undeformed dimensions (right) from Experiment 2: Desktop virtual environment with visual information obscured during replace trials. The vertical axis is in virtual units (v.u.). Shift along each axis was positive indicating that participants generally tended to underestimate distances when navigating to replace the objects, as has been observed previously (Chen et al., 2015; Thompson et al., 2004). Colored arrows indicate the direction of shift difference predicted for each condition. Significance markers denote the outcome of nonparametric Wilcoxon signed rank (one-tailed in predicted directions) and rank sum tests. *p < .05, ***p < .001 [Color figure can be viewed at wileyonlinelibrary.com]

(Compressed: Exp. 1: −4.4697 ± 2.6455 v.u., Exp. 2: −10.9614 ± 4.0599 v.u.; Stretched: Exp. 1:9.3747 ± 3.9241 v.u., Exp. 2:20.0170 ± 4.6564 v.u.; mean ± SEM across participants). This suggests that if anything visual access to walls reduces the appearance of path-dependent shifts in object location memory, though the differences between experiments did not reach significance (Wilcoxon rank sum test, Compressed: W = 591, p = .959; Stretched: W = 505, p = .089).

As in Experiment 1, when the data were analyzed without regards to the boundary of origin, the pattern of replace locations during deformation blocks resembled a rescaling of the familiar object locations that qualitatively matched the rescaling of the environment (Figure S4). Interestingly, this indicates that the appearance of rescaling in the pattern of object replace locations also does not depend on visual access to boundaries at the time of object replacement, contrary to the prediction of some visually-guided models.

Together, these results thus indicate that human spatial memory is dynamically anchored to the boundary of origin in deformed environments even when participants have no visual access to boundaries at the time of object replacement.

2.3 | Experiment 3: Immersive virtual environment with full visual and vestibular information available

Finally, we tested whether human spatial memory is biased by boundary of origin in deformed familiar environments when both vestibular and immersive visual cues are available. To this end, we had a new group of participants complete a fully immersive version of Experiment 1. Participants viewed the virtual room through a stereoscopic head-mounted display (Figure S1c), and their heading and location were tracked as they physically moved about the environment. The experiment comprised two blocks. Each block began with 8 "collect" trials, followed by a sequence of 16 trial pairs consisting of a "replace" trial immediately followed by "collect" trial for the replaced object. Each object was replaced four times in this replace-collect sequence, with each replace trial starting from a position facing the middle of one of the four wall. During the first block, participants learned the locations of four objects as in Experiments 1 and 2, inside a 2.4 m × 2.4 m square virtual room. During the second block, the environment was either stretched (n = 24) or compressed (n = 24; randomly assigned) by 0.4 m along one axis during all replace trials, while remaining undeformed during collect trials. No differences in Block 1 accuracy (distance from correct location; stretched: 0.300 ± 0.023 m; compressed: 0.352 ± 0.026 m; Wilcoxon rank sum test, two-tailed: W = 654, p = .177) or reaction time (stretched: 3.27 ± 0.17 s; compressed: 3.27 ± 0.15 s; Wilcoxon rank sum test, two-tailed: W = 592, p = .942) were observed between participants assigned to the stretched versus compressed conditions, indicating that both groups of participants learned the task equally well.

During the deformation block we again observed a positive shift difference for replace trials in the stretched environment (Wilcoxon signed rank test vs. 0, one-tailed: W = 286, p = .00005) and a negative

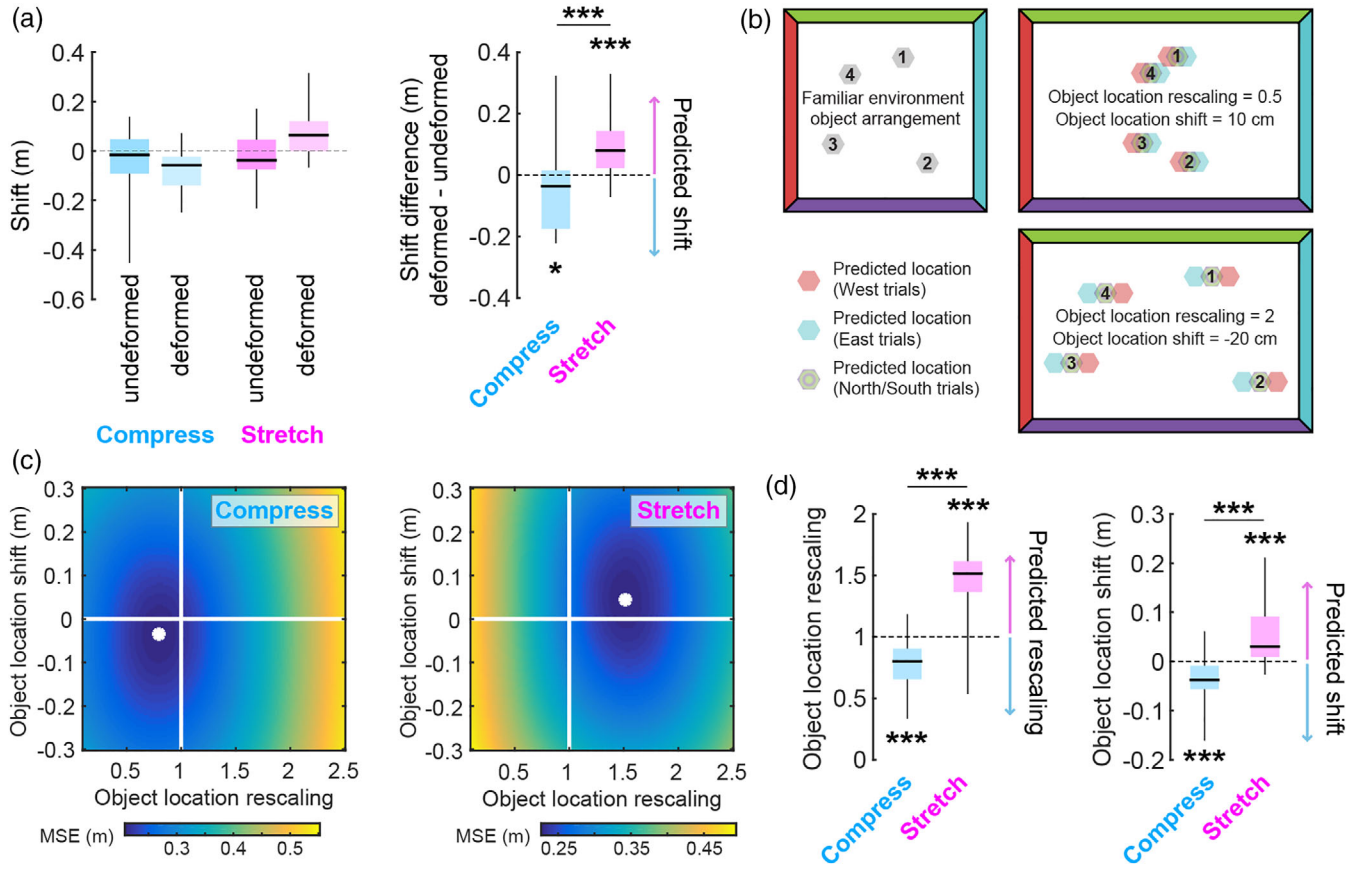

FIGURE 6 Deformations induce path-dependent shifts in human spatial memory when full visual and vestibular information is available. (a) Shift along each axis for each condition (left) and shift difference between deformed and undeformed dimensions (right) from Experiment 3: Immersive virtual environment with full visual and vestibular information available. Unlike previous experiments, no positive early-stopping bias was observed in this smaller immersive environment. (b) Because no evidence for early stopping was observed, we attempted to fit each participant's pattern of deformation block replace locations with a model incorporating both rescaling and/or path-dependent shift dynamics. To this end, we computed the mean square error (MSE) of deformation block replace locations relative to transformed familiar object locations. See Figure S5 for more examples and details. (c) Examples of MSE as a function of rescaling and shift values averaged across all experiments. White dot indicates parameters yielding the minimum MSE for each condition. (d) Distribution of object location rescaling and shift values that minimized MSE across participants in each condition. A hybrid model incorporating both rescaling and path-dependent shifts provides the best fit for both conditions. Colored arrows indicate the direction of shift difference predicted for each condition. Significance markers denote the outcome of nonparametric Wilcoxon signed rank (one-tailed in predicted directions) and rank sum tests. $^{*}p < .05$, $^{***}p < .001$ [Color figure can be viewed at wileyonlinelibrary.com]

shift difference for replace trials in the compressed environment (Wilcoxon signed rank test vs. 0, one-tailed: W = 88, p = .0382) matching our predictions, with a significant difference between conditions (Wilcoxon rank sum test, one-tailed: W = 398, p = .00009; Figures 6a and S2c). No significant difference in shift along undeformed dimensions was observed between stretched and compressed conditions (Wilcoxon rank sum test: W = 600, p = .8126).

As in Experiments 1 and 2, participants on average tended to face away from the boundary of origin when replacing objects (Figure S3). Likewise, when the data were analyzed without regards to the boundary of origin, the pattern of replace locations during deformation blocks resembled a rescaling of the familiar object locations that qualitatively matching the rescaling of the environment (Figure S4). To further examine the relationship between rescaling and path-dependent shift dynamics, we sought to characterize each participant's pattern of deformation block replace locations by fitting a model which incorporated two factors: rescaling and path-dependent shift dynamics. To this end, we computed the mean square error (MSE) of deformation block replace locations relative to transformed familiar object locations across a range of rescaling and shift values (Figure 6b and S5a). Doing so revealed that participants' patterns of responses were best explained by a hybrid model which incorporated both rescaling (Wilcoxon signed rank test vs. 0, one-tailed, compressed: W = 378, p = 2.75e−6, stretched: W = 378, p = 2.75e−6; Wilcoxon rank sum test, one-tailed, compressed versus stretched: W = 404, p = 4.85e−9) and path-dependent shift dynamics (Wilcoxon signed rank test vs. 0, one-tailed, compressed: W = 38, p = 1.40e−4, stretched: W = 345.5, p = 8.40e−5; Wilcoxon rank sum test, one-tailed, compressed vs. stretched: W = 443, p = 2.22e−7) in the predicted directions (Figures 6c,d and S5b). We note that we were unable to perform a similar

analysis in previous experiments as participants tended to stop early when replacing objects regardless of the boundary of origin (Figures 4 and 5); therefore, modeling the patterns of replace locations in Experiments 1 and 2 would require at least one additional early stopping factor, with some dubiousness surrounding how to implement such a component.

Together, these results provide further evidence that human spatial memory is dynamically anchored to the boundary of origin during environmental deformations. We observe dynamic shifts in replace location not only with desktop VR, but also in immersive VR when full vestibular and visual cues are available. Moreover, we provide specific evidence that a hybrid account incorporating both rescaling and path-dependent shift dynamics best explains human spatial memory in deformed environments.

3 | DISCUSSION

Our results show that human spatial memory exhibits a history-dependent anchoring effect. When participants are asked to replace an object in a remembered location in a deformed environment, they choose locations biased by the distance to their boundary of origin. That is, they tend to recapitulate the distance to the boundary of origin, even though this means that they replace the object at inconsistent positions. This finding was replicated in three experimental situations—a desktop virtual environment with localizing visual information available, a desktop virtual environment with localizing visual information obscured, and an immersive virtual environment with localizing visual and vestibular information available. This triple replication indicates that the results are robust and that anchoring dynamics are resilient to variations in the perceptual information available during navigation. Shifts in human spatial memory dependent on boundary of origin were qualitatively similar to dynamic shifts in the grid code of rats freely exploring deformed environments (Keinath et al., 2018). Together, these results suggest the existence of a common mechanism underlying the history-dependent dynamics assayed by both rodent spatial representations and human spatial memory during environmental deformations.

These results build on earlier work showing correspondences between memory-driven behavior in humans and the neural patterns observed in rodent place and grid cells, but move beyond past results in several ways. It has been previously shown that when people are asked to navigate in desktop VR to the remembered locations of objects in stretched versions of familiar environments, their responses qualitatively match the stretching and bifurcations observed in hippocampal place cells (Hartley et al., 2004). Similarly, when participants in immersive VR are asked to walk to an earlier location in the absence of visual cues after navigating through a stretched or compressed environment, they exhibit biases that are consistent with the use of stretched or compressed grid cells for path integration (Chen et al., 2015). Relatedly, a recent study using immersive VR in square and trapezoidal environments found that object replace locations and distance estimations were biased in a manner that could be predicted based on the inhomogeneities of rodent grid cells in such environments (Bellmund et al., 2020). In the current study, we tested a specific prediction: that the remembered locations of objects would undergo trajectory-dependent shifts in deformed environments. At an algorithmic level, this prediction follows from the hypothesis that the path-integrated self-localization estimate would be reset when a familiar boundary is encountered. At an implementation level, this prediction was derived from a computational model where grid phase is dynamically anchored to the most recently-contacted boundary, possibly through input from border cells. We previously showed that many implementation-level predictions of this account were borne out in existing grid cell data sets (Keinath et al., 2018). Here we show even stronger evidence for this account, by demonstrating that these predictions are borne out in human behavior, across three experiments using both desktop and immersive VR.

These findings are important for two reasons. First, they provide additional evidence for a strong and specific correspondence between neural effects observed in rodent grid and place cells and memory effects observed in human behavior during environmental deformations. Such correspondences between cellular-level phenomena and behavior are far from guaranteed—in many cases predictions generated on the basis of subsets of neuronal representations are not realized behaviorally (Ekstrom et al., 2020; Jeffery et al., 2003; Krakauer et al., 2017; Warren, 2019; Zhao, 2018). Second, in contrast to previous studies of deformation effects, our results cannot be easily explained in terms of scaling deformations of the cognitive map. Rather, our results suggest that a primary function of place and grid cells is to integrate distances from particular point of reference. In most ecological situations, this function would lead to an accurate and consistent representation of where the navigator is in space, and hence an accurate cognitive map. In the case of a deformed environment, however, the system must adjudicate between maintaining the coherence of the global coordinate system through scaling deformations and maintaining the fidelity of the spatial metric by shifting the map based on anchoring to some external cue (in this case the most recently encountered boundary). Previous studies have highlighted evidence for scaling deformations (Barry et al., 2007; Chen et al., 2015; Hartley et al., 2004; Munn et al., 2020; Stensola et al., 2012). Consistent with the results of these studies, we find that the average pattern of replace locations resembles a rescaling which qualitatively matches the deformation of the environment (Chen et al., 2015; Hartley et al., 2004). However, when we break down the data based on the boundary of origin, we observe robust evidence that the spatial metric is dynamically dependent on the starting point of each trial, and that distance to this starting point is preserved to a greater degree than expected on the basis of a rescaling deformation alone. Moreover, when we specifically fit a two-factor model to our immersive VR data, we find clear evidence of concurrent rescaling and path-dependent shift effects, suggesting an integrative interaction between dynamically-anchored path integration and visual cues (Cheng, Shettleworth, Huttenlocher, & Rieser, 2007). Thus, a static

coordinate transformation alone cannot completely explain the data; dynamic shifts must play a role.

One limitation of the current study was that replace trials initiated from each boundary always began at the same starting location. As such, starting location and boundary of origin were confounded. Thus, we cannot say for certain that the dynamic anchoring mechanism we observe anchors to boundaries. Other spatially informative non-boundary cues or experimental regularities could, in theory, also serve as dynamic anchors. Indeed, behavioral (Etienne, Boulens, Maurer, Rowe, & Siegrist, 2000; Etienne & Jeffery, 2004; Zhao & Warren, 2015) and neural (Jayakumar et al., 2019; Pérez-Escobar, Kornienko, Latuske, Kohler, & Allen, 2016; Save, Cressant, Thinus-Blanc, & Poucet, 1998) evidence indicates that punctate landmarks can reset and recalibrate path integration. Moreover, neural correlates of a vectoral landmark representation which could mediate such dynamics have been observed throughout the hippocampal formation (Deshmukh & Knierim, 2011, 2013; Høydal, Skytøen, Andersson, Moser, & Moser, 2019). Nevertheless, growing evidence indicates boundaries play a privileged role in shaping spatial representations and spatial memory alike (Doeller & Burgess, 2008; Doeller, King, & Burgess, 2008; Keinath et al., 2017; Weiss et al., 2017). Similarly, it remains an open question whether the dynamic biases we observe during deformations are a product of a continuously updated self-localization process, or instead reflect carrying out a previously established route. In our experiments, objects were always collected from random starting locations to minimize the likelihood that they might learn a fixed replacement trajectory. Nevertheless, participants experienced replace trials in the familiar arrangement prior to deformation blocks, and this experience may have influenced their trajectories in subsequent replacement blocks.

The implementation-level mechanism by which environmental deformations induce shifts in human memory has not been established from empirical data. The predictions tested here were derived from a neural network model in which the phase of the grid code, thought to reflect a self-localization estimate updated via self-motion information, was reset upon encountering a familiar boundary. We previously showed that many implementation-level predictions of this model were borne out in existing rodent grid cell data sets (Keinath et al., 2018). Neuroimaging and neural recording data have established the existence of a grid cell network in humans with striking representational parallels to the networks observed in rodents (Doeller, Barry, & Burgess, 2010; He & Brown, 2019; Jacobs et al., 2013; Julian, Keinath, Frazzetta, & Epstein, 2018; Kunz et al., 2019), including the appearance of rescaling (Nadasdy et al., 2017). Thus, it is possible that dynamic shifts in grid phase directly mediate boundary-anchored shifts in human spatial memory. Nevertheless, the purpose and representational content of the grid code, as well as its relationship to path integration, are currently a topic of much debate (Burak & Fiete, 2009; Bush et al., 2015; Dordek, Soudry, Meir, & Derdikman, 2016; McNaughton et al., 2006; Stachenfeld, Botvinick, & Gershman, 2017), and the behavioral predictions of this account could be realized through a variety of implementations which do or do not include a grid code component. Thus while a growing literature supports the correspondence of cross-species grid coding, as well as a general concordance between deformations induced by environmental geometry in both grid coding and spatial memory (Bellmund et al., 2020; Chen et al., 2015), the precise mechanistic basis of these effects remains to be resolved.

In sum, we have shown that human spatial memory in deformed environments exhibits a history-dependent anchoring effect which parallels the dynamic anchoring of grid cells to recently encountered boundaries. This anchoring is robust to a variety of visual and vestibular conditions, and cannot be accounted for by a static transformation of a navigator's cognitive map. These results have important implications for human spatial memory and its relationship with hippocampal spatial representations, and raise additional questions about the specific mechanisms which might link the two.

4 | METHODS

4.1 | Participants

Forty-nine participants gave written consent and were paid for participating in Experiment 1, 53 for Experiment 2, and 48 for Experiment 3. One participant from Experiment 1 and four participants from Experiment 2 were excluded for performing worse than chance by the end of the last familiar block. An additional participant was excluded from Experiment 2 as an outlier (shift score > 3 *SD* above the mean, in the predicted direction), leaving a final count of 48 participants in Experiment 1 (31 female, mean age 23.5, age range 18–44), 48 in Experiment 2 (30 female, mean age 22.4, age range 18–33), and 48 in Experiment 3 (38 female, mean age 22.9, age range 18–44), with 24 participants in each experimental condition. Sample size was chosen prior to conducting all experiments to be double the number of participants in prior experiments studying similar effects (Chen et al., 2015). All participants provided informed consent in accordance with the Institutional Review Board of the University of Pennsylvania.

4.2 | Experimental protocols

4.2.1 | Experiment 1: Desktop virtual environment with full visual information available

We used Source SDK Hammer Editor (http://www.valvesoftware.com, Valve Software, Bellevue, WA) to construct virtual reality environments that were rendered and displayed from the first person-perspective using the commercial game software Portal (http://www.valvesoftware.com, Valve Software, Bellevue, WA). The environment was displayed on a 27-in. LG monitor (resolution: 1920 × 1080) and participants were seated roughly 50 cm from the screen. Participants learned the locations of target objects inside a virtual environment, using the learning procedure described in the main text and illustrated in Figure 2. Participants moved through the environment by using their right hand to operate arrow keys to move forward or backwards

and turn left or right. During the replace phase, participants navigated to their remembered object location and pressed the "r" key with their left hand to register their response. Virtual heading and location were recorded every 100 ms.

The familiar environment was a square virtual arena, with no ceiling. Each boundary wall was 116 virtual units (vu) in length × 5.6 vu in height relative to a simulated eye-level of 4 vu. One virtual unit corresponds to 0.3048 real-world meters (1 ft). The four target objects were a radiator, a lamp, an oil drum, and a cake. At the start of each block, participants collected each target object in pseudo-random order twice without any interspersed replace trials. They then performed 16 replace trials (4 for each object, in pseudo-random order), each of which was immediately followed by a collect trial for the same object to provide feedback. The instructions for each trial (either "Collect" or "Replace," followed by the target object name) were displayed in the center of the screen for the entirety of the trial. During each "collect" trial, only the to-be-collected object was present in the room. During "replace" trials, no objects were present. The same texture was applied to all walls. Distal cues, in the form of the sun, sky, and a mountain range, surrounded the arena (Figure S1). These distal cues were rendered at infinity, thus providing orientation information but no cues to location.

Participants completed two blocks, a familiar block followed by a deformation block. Only replace trials differed between blocks. The environment used in replace trials in the deformation block was either stretched 50% along one-dimension relative the familiar square environment (width 174 vu × length 116 vu) or compressed 50% (width 58 vu x length 116 vu). To create these deformed environments, the floor, wall, and ceiling textures were not rescaled, but were instead truncated (during compressions) or continued to tile the new space (during stretches). Ten participants noticed a difference between the original and the deformed environment.

4.2.2 | Experiment 2: Desktop virtual environment with visual information obscured during replace trials

The design and procedures were similar to that of Experiment 1, except as described below.

The familiar environment was a square virtual room. Each wall was textured with a unique wallpaper to provide orientational cues. The floor was also repetitively textured to provide optic flow information but the floor texture provided no cues to location inside the environment. Each boundary wall was 116 virtual units (vu) in length and 19 vu in height relative to a simulated eye-level of 4 vu. The environment was completely enclosed by the walls and ceiling (Figure S1).

Participants completed three blocks. In the first block, the environment was a square, and visual cues were always visible. In the second block, the environment was also a square, and visual cues during replace trials (but not collect trials) were masked by a dense fog once the participant traveled at least 3.1 vu away from their starting location. The fog fully saturated at 12.5 vu, occluding all visual cues beyond this radius. All objects were located at least 30 vu from all boundaries. In the third block (deformation block), visual cues were also masked by dense fog upon movement from the initial position and the familiar room was replaced by a rectangular room which was either stretched 50% from the original square along one axis (width 174 vu x length 116 vu) or compressed 50% (width 58 vu x length 116 vu). To create these deformed environments, the floor, wall, and ceiling textures were not rescaled, but were instead truncated (for compressions) or continued to tile the new space (for stretches). Eleven participants noticed a difference between the original and the deformed environment.

4.2.3 | Experiment 3: Immersive virtual environment with full visual and vestibular information available

The design and procedures for Experiment 3 were similar to those of Experiment 1, except as described here. We used Unity game engine version 5.6 (https://unity3d.com, Unity Technologies, San Francisco, CA) to construct and render immersive virtual reality rooms via the stereoscopic HTC Vive head-mounted display and position tracker (resolution of 1,080 × 1,200 per eye; https://www.vive.com/, HTC with technology by the Valve Corporation, New Taipei City, Taiwan). Responses during the replace phase were collected by participants pressing the "trigger" key of a wireless HTC Vive controller with their dominant hand. Participants could freely move their head and walk around the environment. Their heading and location were recorded every 100 ms. No participants complained of motion sickness during or after the experiment.

The familiar environment was a square virtual room, measuring 2.4 m in length x 2.4 m in width x 2.5 m in height. The positions of 2 (north–south) virtual walls matched 2 of the physical tracking room walls, the remaining 2 (east–west) unmatched virtual walls were displaced during deformations. All walls were textured a charcoal grey. The floor and ceiling were textured a lighter grey. A light grey floor-to-ceiling 0.1 m wide x 0.1 m long column was nestled in each corner to deter participants from contacting the tracking equipment (Figure S1).

Participants completed two blocks, a familiar block followed by a deformation block. Only replace trials differed between blocks. The environment used during replace trials of the deformation block was either stretched along one-dimension (east–west) by displacing one or both unmatched walls and their neighboring columns (width 2.8 m x length 2.4 m) or compressed along this dimension (width 2.0 m x length 2.4 m). Between blocks, the display was rendered solid black for 5 s with the instructions "wait for next trial" displayed in the bottom center of the visual field.

Because participants could no longer be teleported between trials, they were instructed to move before each trial to face and nearly touch the center of one of the four walls as indicated by a floating black arrow. To ensure that the participant did not see any walls move during deformation trials, the displaced wall depended on the starting position for that trial. If the trial started from the east wall, then the

west wall was displaced by 0.4 m. If the trial started from the west wall, then the east wall was displaced by 0.4 m. If the trial started from either the north or the south walls, then both the east and west walls were displaced by 0.2 m each. From all starting positions, the instantaneous displacement of walls was not visible. No participant noticed the manipulation.

The complete set of target objects was a red sphere, a blue cube, a green cylinder, and a purple capsule. Object locations were all within 0.4 m of the center of the familiar environment. All objects were presented on the same grey 1.5 m tall pedestal in order to raise them to approximately eye level (Figure S1). The target objects for each trial were selected in pseudo-random order. The instructions (either "Collect the" or "Replace the" followed by the target object name in text matching the color of the target object, or "Go to Arrow" to begin the next trial) were displayed in the bottom center of the visual field for the entirety of all trials.

4.3 | Analysis

All recorded data were imported into MATLAB (MathWorks) and analyzed using custom written scripts.

4.3.1 | Object replace location analysis

As described in the main text and Figure 3, to test whether the replaced locations of objects depended on the starting boundary, we first aligned all four objects by subtracting their median replaced locations. Next, for each axis (north–south and east–west) we calculated the displacement along that axis between the median replace locations when starting from one boundary (north or east) minus the opposing boundary (south or west). Lastly, we computed the difference in shift measured along the deformed and undeformed dimensions as the final measure of interest. Medians were chosen as the measure of central tendency to mitigate the effect of outliers in replaced locations.

4.3.2 | Statistics

All statistical tests were two-tailed (unless otherwise noted) nonparametric tests with the particular test noted accompanying each result. Given the typically long-tailed distribution of the shift data, nonparametric tests were chosen as these tests do not assume a particular shape of the tested distributions. W-statistics were reported for all Wilcoxon signed rank and rank sum tests. All box-and-whisker plots indicate the minimum to maximum (whisker), the first to third quartile range (box), and the median (line) of the distribution.

ACKNOWLEDGMENTS

We gratefully acknowledge support from NSF grant PHY-1734030 (VB), NIH grants EY022350 and EY027047 (RAE), and NSF IGERT grant 0966142 (ATK). VB was also partially supported by the Honda Research Institute Curious-Minded Machines program and the Aspen Center for Physics (Aspen, Colorado; NSF grant PHY-1607611) during this time.

CONFLICT OF INTEREST

The authors declare no competing conflicts of interest.

DATA AVAILABILITY STATEMENT

Data and custom MATLAB scripts implementing all analyses are publicly available at https://github.com/akeinath/HumanMemory_EnvironmentalDeformations.

ORCID

Alexandra T. Keinath https://orcid.org/0000-0003-1622-7835

REFERENCES

Barry, C., Hayman, R., Burgess, N., & Jeffery, K. J. (2007). Experience-dependent rescaling of entorhinal grids. *Nature Neuroscience*, *10*, 682–684. https://doi.org/10.1038/nn1905

Bellmund, J. L. S., de Cothi, W., Ruiter, T. A., Nau, M., Barry, C., & Doeller, C. F. (2020). Deforming the metric of cognitive maps distorts memory. *Nature Human Behaviour*, *4*, 177–188. https://doi.org/10.1038/s41562-019-0767-3

Burak, Y., & Fiete, I. R. (2009). Accurate path integration in continuous attractor network models of grid cells. *PLoS Computational Biology*, *5*, e1000291. https://doi.org/10.1371/journal.pcbi.1000291

Bush, D., Barry, C., Manson, D., & Burgess, N. (2015). Using grid cells for navigation. *Neuron*, *87*, 507–520. https://doi.org/10.1016/j.neuron.2015.07.006

Bush, D., & Burgess, N. (2014). A hybrid oscillatory interference/continuous attractor network model of grid cell firing. *The Journal of Neuroscience*, *34*, 5065–5079. https://doi.org/10.1523/JNEUROSCI.4017-13.2014

Chen, G., Lu, Y., King, J. A., Cacucci, F., & Burgess, N. (2019). Differential influences of environment and self-motion on place and grid cell firing. *Nature Communications*, *10*, 630. https://doi.org/10.1038/s41467-019-08550-1

Chen, X., He, Q., Kelly, J. W., Fiete, I. R., & McNamara, T. P. (2015). Bias in human path integration is predicted by properties of grid cells. *Current Biology*, *25*, 1771–1776. https://doi.org/10.1016/j.cub.2015.05.031

Cheng, K., Shettleworth, S. J., Huttenlocher, J., & Rieser, J. J. (2007). Bayesian integration of spatial information. *Psychological Bulletin*, *133*, 625–637. https://doi.org/10.1037/0033-2909.133.4.625

Cheung, A., Ball, D., Milford, M., Wyeth, G., & Wiles, J. (2012). Maintaining a cognitive map in darkness: The need to fuse boundary knowledge with path integration. *PLoS Computational Biology*, *8*, e1002651. https://doi.org/10.1371/journal.pcbi.1002651

Deshmukh, S. S., & Knierim, J. J. (2011). Representation of non-spatial and spatial information in the lateral entorhinal cortex. *Frontiers in Behavioral Neuroscience*, *5*, 69. https://doi.org/10.3389/fnbeh.2011.00069

Deshmukh, S. S., & Knierim, J. J. (2013). Influence of local objects on hippocampal representations: Landmark vectors and memory. *Hippocampus*, *23*, 253–267. https://doi.org/10.1002/hipo.22101

Doeller, C. F., Barry, C., & Burgess, N. (2010). Evidence for grid cells in a human memory network. *Nature*, *463*, 657–661. https://doi.org/10.1038/nature08704

Doeller, C. F., & Burgess, N. (2008). Distinct error-correcting and incidental learning of location relative to landmarks and boundaries. *Proceedings of the National Academy of Sciences of the United States of America*, *105*, 5909–5914. https://doi.org/10.1073/pnas.0711433105

Doeller, C. F., King, J. A., & Burgess, N. (2008). Parallel striatal and hippocampal systems for landmarks and boundaries in spatial memory.

Proceedings of the National Academy of Sciences of the United States of America, *105*, 5915–5920. https://doi.org/10.1073/pnas.0801489105

Dordek, Y., Soudry, D., Meir, R., & Derdikman, D. (2016). Extracting grid cell characteristics from place cell inputs using non-negative principal component analysis. *eLife*, *5*, e10094. https://doi.org/10.7554/eLife.10094

Ekstrom, A. D., Harootonian, S. K., & Huffman, D. J. (2020). Grid coding, spatial representation, and navigation: Should we assume an isomorphism? *Hippocampus*, *30*, 422–432. https://doi.org/10.1002/hipo.23175

Epstein, R. A., Patai, E. Z., Julian, J. B., & Spiers, H. J. (2017). The cognitive map in humans: Spatial navigation and beyond. *Nature Neuroscience*, *20*, 1504–1513. https://doi.org/10.1038/nn.4656

Etienne, A. S., Boulens, V., Maurer, R., Rowe, T., & Siegrist, C. (2000). A brief view of known landmarks reorientates path integration in hamsters. *Naturwissenschaften*, *87*, 494–498. https://doi.org/10.1007/s001140050766

Etienne, A. S., & Jeffery, K. J. (2004). Path integration in mammals. *Hippocampus*, *14*, 180–192. https://doi.org/10.1002/hipo.10173

Fiete, I. R., Burak, Y., & Brookings, T. (2008). What grid cells convey about rat location. *The Journal of Neuroscience*, *28*, 6858–6871. https://doi.org/10.1523/JNEUROSCI.5684-07.2008

Gallistel, C. R. (1990). *The organization of learning*. Cambridge, MA: Bradform Books/MIT Press.

Hafting, T., Fyhn, M., Molden, S., Moser, M.-B., & Moser, E. I. (2005). Microstructure of a spatial map in the entorhinal cortex. *Nature*, *436*, 801–806. https://doi.org/10.1038/nature03721

Hardcastle, K., Ganguli, S., & Giocomo, L. M. (2015). Environmental boundaries as an error correction mechanism for grid cells. *Neuron*, *86*, 827–839. https://doi.org/10.1016/j.neuron.2015.03.039

Hartley, T., Trinkler, I., & Burgess, N. (2004). Geometric determinants of human spatial memory. *Cognition*, *94*, 39–75. https://doi.org/10.1016/j.cognition.2003.12.001

He, Q., & Brown, T. I. (2019). Environmental barriers disrupt grid-like representations in humans during navigation. *Current Biology*, *29*, 2718–2722.e3. https://doi.org/10.1016/j.cub.2019.06.072

Høydal, Ø. A., Skytøen, E. R., Andersson, S. O., Moser, M.-B., & Moser, E. I. (2019). Object-vector coding in the medial entorhinal cortex. *Nature*, *568*, 400–404. https://doi.org/10.1038/s41586-019-1077-7

Jacobs, J., Weidemann, C. T., Miller, J. F., Solway, A., Burke, J. F., Wei, X.-X., … Kahana, M. J. (2013). Direct recordings of grid-like neuronal activity in human spatial navigation. *Nature Neuroscience*, *16*, 1188–1190. https://doi.org/10.1038/nn.3466

Jayakumar, R. P., Madhav, M. S., Savelli, F., Blair, H. T., Cowan, N. J., & Knierim, J. J. (2019). Recalibration of path integration in hippocampal place cells. *Nature*, *566*, 533–537. https://doi.org/10.1038/s41586-019-0939-3

Jeffery, K. J., Gilbert, A., Burton, S., & Strudwick, A. (2003). Preserved performance in a hippocampal-dependent spatial task despite complete place cell remapping. *Hippocampus*, *13*, 175–189. https://doi.org/10.1002/hipo.10047

Julian, J. B., Keinath, A. T., Frazzetta, G., & Epstein, R. A. (2018). Human entorhinal cortex represents visual space using a boundary-anchored grid. *Nature Neuroscience*, *21*, 191–194. https://doi.org/10.1038/s41593-017-0049-1

Keinath, A. T., Epstein, R. A., & Balasubramanian, V. (2018). Environmental deformations dynamically shift the grid cell spatial metric. *eLife*, *7*, e38169. http://dx.doi.org/10.7554/elife.38169.

Keinath, A. T., Julian, J. B., Epstein, R. A., & Muzzio, I. A. (2017). Environmental geometry aligns the hippocampal map during spatial reorientation. *Current Biology*, *27*, 309–317. https://doi.org/10.1016/j.cub.2016.11.046

Krakauer, J. W., Ghazanfar, A. A., Gomez-Marin, A., MacIver, M. A., & Poeppel, D. (2017). Neuroscience needs behavior: Correcting a reductionist bias. *Neuron*, *93*, 480–490. https://doi.org/10.1016/j.neuron.2016.12.041

Krupic, J., Bauza, M., Burton, S., Barry, C., & O'Keefe, J. (2015). Grid cell symmetry is shaped by environmental geometry. *Nature*, *518*, 232–235. https://doi.org/10.1038/nature14153

Krupic, J., Bauza, M., Burton, S., & O'Keefe, J. (2018). Local transformations of the hippocampal cognitive map. *Science (80-)*, *359*, 1143–1146. https://doi.org/10.1126/science.aao4960

Kunz, L., Maidenbaum, S., Chen, D., Wang, L., Jacobs, J., & Axmacher, N. (2019). Mesoscopic neural representations in spatial navigation. *Trends in Cognitive Sciences*, *23*, 615–630. https://doi.org/10.1016/j.tics.2019.04.011

McNaughton, B. L., Barnes, C. A., Gerrard, J. L., Gothard, K., Jung, M. W., Knierim, J. J., … Weaver, K. L. (1996). Deciphering the hippocampal polyglot: The hippocampus as a path integration system. *The Journal of Experimental Biology*, *199*, 173–185.

McNaughton, B. L., Battaglia, F. P., Jensen, O., Moser, E. I., & Moser, M.-B. (2006). Path integration and the neural basis of the "cognitive map.". *Nature Reviews Neuroscience*, *7*, 663–678. https://doi.org/10.1038/nrn1932

Munn, R. G. K., Mallory, C. S., Hardcastle, K., Chetkovich, D. M., & Giocomo, L. M. (2020). Entorhinal velocity signals reflect environmental geometry. *Nature Neuroscience*, *23*(2), 239–251. http://dx.doi.org/10.1038/s41593-019-0562-5.

Nadasdy, Z., Nguyen, T. P., Török, Á., Shen, J. Y., Briggs, D. E., Modur, P. N., & Buchanan, R. J. (2017). Context-dependent spatially periodic activity in the human entorhinal cortex. *Proceedings of the National Academy of Sciences*, *114*, E3516–E3525. https://doi.org/10.1073/pnas.1701352114

O'Keefe, J., & Burgess, N. (1996). Geometric determinants of the place fields of hippocampal neurons. *Nature*, *381*, 425–428. https://doi.org/10.1038/381425a0

O'Keefe, J., & Dostrovsky, J. (1971). The hippocampus as a spatial map. Preliminary evidence from unit activity in the freely-moving rat. *Brain Research*, *34*, 171–175. https://doi.org/10.1016/0006-8993(71)90358-1

O'Keefe, J., & Nadel, L. (1978). *The hippocampus as a cognitive map*. Oxford: Clarendon Press.

Ocko, S. A., Hardcastle, K., Giocomo, L. M., & Ganguli, S. (2018). Emergent elasticity in the neural code for space. *Proceedings of the National Academy of Sciences of the United States of America*, *115*, E11798–E11806. https://doi.org/10.1073/pnas.1805959115

Pérez-Escobar, J. A., Kornienko, O., Latuske, P., Kohler, L., & Allen, K. (2016). Visual landmarks sharpen grid cell metric and confer context specificity to neurons of the medial entorhinal cortex. *eLife*, *5*, e16937. https://doi.org/10.7554/eLife.16937

Raudies, F., & Hasselmo, M. E. (2015). Differences in visual-spatial input may underlie different compression properties of firing fields for grid cell modules in medial Entorhinal cortex. *PLoS Computational Biology*, *11*, e1004596. https://doi.org/10.1371/journal.pcbi.1004596

Save, E., Cressant, A., Thinus-Blanc, C., & Poucet, B. (1998). Spatial firing of hippocampal place cells in blind rats. *The Journal of Neuroscience*, *18*, 1818–1826.

Savelli, F., Luck, J., & Knierim, J. J. (2017). Framing of grid cells within and beyond navigation boundaries. *eLife*, *6*, e21354. https://doi.org/10.7554/eLife.21354

Savelli, F., Yoganarasimha, D., & Knierim, J. J. (2008). Influence of boundary removal on the spatial representations of the medial entorhinal cortex. *Hippocampus*, *18*, 1270–1282. https://doi.org/10.1002/hipo.20511

Sheynikhovich, D., Chavarriaga, R., Strösslin, T., Arleo, A., & Gerstner, W. (2009). Is there a geometric module for spatial orientation? Insights from a rodent navigation model. *Psychological Review*, *116*, 540–566. https://doi.org/10.1037/a0016170

Stachenfeld, K. L., Botvinick, M. M., & Gershman, S. J. (2017). The hippocampus as a predictive map. *Nature Neuroscience*, *20*, 1643–1653. https://doi.org/10.1038/nn.4650

Stensola, H., Stensola, T., Solstad, T., Frøland, K., Moser, M.-B., & Moser, E. I. (2012). The entorhinal grid map is discretized. *Nature*, *492*, 72–78. https://doi.org/10.1038/nature11649

Stensola, T., Stensola, H., Moser, M.-B., & Moser, E. I. (2015). Shearing-induced asymmetry in entorhinal grid cells. *Nature*, *518*, 207–212. https://doi.org/10.1038/nature14151

Thompson, W. B., Willemsen, P., Gooch, A. A., Creem-Regehr, S. H., Loomis, J. M., & Beall, A. C. (2004). Does the quality of the computer graphics matter when judging distances in visually immersive environments? *Presence Teleoperators and Virtual Environments*, *13*, 560–571. https://doi.org/10.1162/1054746042545292

Warren, W. H. (2019). Non-euclidean navigation. *The Journal of Experimental Biology*, *222*, jeb187971. https://doi.org/10.1242/jeb.187971

Weiss, S., Talhami, G., Gofman-Regev, X., Rapoport, S., Eilam, D., & Derdikman, D. (2017). Consistency of spatial representations in rat entorhinal cortex predicts performance in a reorientation task. *Current Biology*, *27*, 3658–3665.e4. https://doi.org/10.1016/j.cub.2017.10.015

Zhao, M. (2018). Human spatial representation: What we cannot learn from the studies of rodent navigation. *Journal of Neurophysiology*, *120*, 2453–2465. https://doi.org/10.1152/jn.00781.2017

Zhao, M., & Warren, W. H. (2015). How you get there from here: Interaction of visual landmarks and path integration in human navigation. *Psychological Science*, *26*, 915–924. https://doi.org/10.1177/0956797615574952

SUPPORTING INFORMATION

Additional supporting information may be found online in the Supporting Information section at the end of this article.

How to cite this article: Keinath AT, Rechnitz O, Balasubramanian V, Epstein RA. Environmental deformations dynamically shift human spatial memory. *Hippocampus*. 2020; 1–13. https://doi.org/10.1002/hipo.23265